Journal of proteome research

Article

pubs.acs.org/jpr

Multiple Reaction Monitoring of Multiple Low-Abundance Transcription Factors in Whole Lung Cancer Cell Lysates

Jun Seok Kim,[†] Youngju Lee,[†] Min Young Lee,[‡] Jihye Shin,[†] Jung Min Han,[⊥,#] Eun Gyeong Yang,[†] Myeong-Hee Yu,[†] Sunghoon Kim,[⊥,#] Daehee Hwang,[‡,§,∥] and Cheolju Lee*[,†]

[†]Theragnosis Research Center, Korea Institute of Science and Technology, Seoul, Korea

[‡]School of Interdisciplinary Bioscience and Bioengineering, POSTECH, Pohang, Korea

[§]Integrative Biosciences and Biotechnology, POSTECH, Pohang, Korea

[∥]Department of Chemical Engineering, POSTECH, Pohang, Korea

[⊥]Medicinal Bioconvergence Research Center, Seoul National University, Seoul, Korea

[#]WCU Department of Molecular Medicine and Biopharmaceutical Sciences, Seoul National University, Suwon, Korea

Supporting Information

ABSTRACT: Lung cancer-related transcription factors (TFs) were identified by integrating previously reported genomic, transcriptomic, and proteomic data and were quantified by multiple reaction monitoring (MRM) in various cell lines. All experiments were performed without affinity depletion or subfractionation of cell lysates. Since the target proteins were expected to be present in low abundance, we experimentally optimized MRM transition parameters with chemically synthesized peptides. Quantitation was based on stable isotope-labeled standard peptides (SIS peptides). Out of 288 MRM measurements (36 peptides representing 28 TFs × 8 cell lines), 241 were successfully obtained within a quantitation limit of 15 amol, 221 measurements (91.7%) showed coefficients of variation (CVs) of ≤20%, and 149 (61.8%) showed CVs of ≤10%, quantifying as low as 19.4 amol/μg protein for STAT2 with a CV of 6.3% in an A549 cell. Comparisons between MRM measurements and levels of the corresponding mRNAs revealed linear, nonlinear, or no relationship between protein and mRNA levels, indicating the need for an MRM assay. An integrative analysis of MRM and gene expression profiles from doxorubicin-resistant H69AR and sensitive H69 cells further showed that 14 differentially expressed TFs, such as STAT1 and SMAD4, regulated genes associated with drug resistance and cell differentiation-related processes. Thus, the analytical performance of MRM for the quantitation of low abundance TFs suggests its usefulness for biological application.

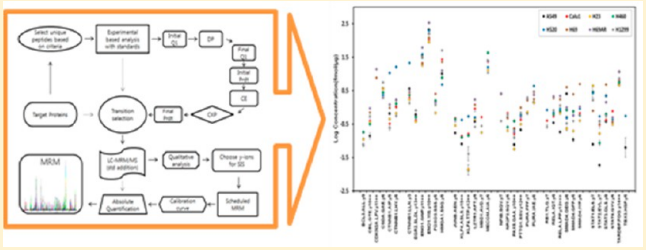

KEYWORDS: *TF, MRM, transition parameters, doxorubicin, drug-resistance*

INTRODUCTION

For several decades, immunobased assays, such as ELISA, Western blot, FACS and other immunoassay methods, have been widely utilized in clinical laboratories for the discovery and validation of the biomarkers.[1−3] This long period of study with immunoassays has provided much important experimental knowledge and diagnostic information on patients. In addition, fluorescent spectroscopic detection with these assays has provided very high sensitivity for low-abundance targets.[4] Thus, these assays are well-accepted in clinical research fields. However, these assays are restricted to small number of targets, and the results are very dependent on the quality of the antibodies for each target protein. Also, the cost of generating a highly efficient antibody for a newly targeted biomarker is quite high.

The application of mass spectroscopic (MS) techniques, particularly liquid chromatography−tandem mass spectrometry (LC−MS/MS), to peptide and protein research in the mid-1990s opened a new field termed MS-based proteomics.[5] This technology is very powerful in that it can identify and quantify the peptide sequences of the target proteins in a complex mixture.[6,7] Recently developed instruments, with a fast scan speeds, multiplexing capabilities, high resolution, and accurate mass measurement capabilities, have increased the applications of MS in proteomics research. Sample concentration and selective target enrichment facilitate the application to low-abundance proteins.[8,9] In addition, the use of data independent acquisition (DIA) in MS improves the selectivity for the low targets.[10] However, these complicated procedures require expert knowledge and skill. Moreover, the quantitative and even qualitative information obtained from the techniques may give different analytical results between laboratories.

Received: December 4, 2012
Published: April 15, 2013

dx.doi.org/10.1021/pr3011414 | J. Proteome Res. 2013, 12, 2582−2596

The development of multiple reaction monitoring (MRM) with triple quadrupole (QQQ) MS systems as an attractive biomarker quantitation tool has led to a new area of analytical research.[11−14] The advantages of MRM are varied by targeting and quantifying analytes of interest. MRM has strengthened genomics-driven findings.[15] Although massive genomic data continue to flood into diagnostic laboratories, absolute quantitation at the protein level is essential since the expression level of a protein in a biological sample is critical in disease.[16,17] Nano-LC interfaced to MRM-MS enables multiple low-abundance targets to be simultaneously quantified.[18,19] This is very important since various targets play critical roles in a disease.[18] MRM is also a rapid, selective, sensitive and cost-effective bioanalytical strategy. Like LC−MS/MS, the sample analysis time is very fast once the instrumental parameters, such as collisional energy (CE), declustering potential (DP), retention time (t_R), target transition, etc., have been optimized.[18] By optimizing DP and CE, ionization and fragmentation efficiencies can be improved for sensitive MRM assay. The scheduling algorithms in recent QQQ instruments enable over 1000 targets to be scanned in predefined time zones during a single run.[20] This feature makes this technique superior to ELISAs, which need more than a day to analyze 96 target proteins. Moreover, the MRM process does not require any antibody for most experiments, since it requires only the transitions of the proteotypic peptides for the target proteins. Another advantage of QQQ is the selectivity of the user-defined transitions. In QQQ, there are basically two mass filtering systems located in the first and third quadrupoles. The first quadrupole selects the precursor ions (intact peptides) and the third quadrupole selects the product ions (after fragmentation of the peptides in the second quadrupole, the collision cell). This selective process filters out undefined transitions and chemical noise and allows the quantitation of low-abundance targets, resulting in higher sensitivities. Therefore, high speed multiplexed MRM makes it possible to analyze low-abundance targets in large numbers of real samples, which is required for biomarker validation.

In this study, we used an MRM assay for multiplexed analysis of low-abundance transcription factors (TFs) in various lung cancer cells. Lung cancer has the second highest mortality rate and the highest death rate among cancers.[21] Chemotherapy using doxorubicin (DOX) and its combination with other agents has been the most effective treatment for small cell lung cancer patients.[22,23] However, lung cancer patients may possess or develop resistance to DOX. Several DOX resistance factors have been proposed, including (i) ABC transporters (MDR1/ABCB1, MRP1/ABCC1etc.),[24] (ii) glutathione-*S*-transferase (GSTpi),[25,26] and (iii) metallthionein.[27] However, determination of the signaling pathways and/or the TFs inducing these resistance factors is still elusive. Proteomic analysis of TFs can confirm the association of these TFs with DOX resistance in lung cancer. However, the abundance of most TFs in lung cancer cells is low, compelling researchers to reduce the complexity of samples by affinity isolation or fractionation.[28,29] Here, without affinity depletion and fractionation of lung cancer-related cell lines, we have quantified multiple low-abundance TFs by using a nano-LC−MRM assay. Our results suggest that diagnostic and prognostic applications of lung cancer-related TFs are possible if an MRM assay is used.

EXPERIMENTAL PROCEDURES

Selection of Proteotypic Peptides for MRM Assays

We generated target peptide lists for our MRM assay by considering the following peptide selection criteria: peptides containing 6 ≤ amino acids ≤ 20mers were chosen first. Since m/z 1250 is the maximum scan range of the ABI QTrap5500 triple quadrupole mass spectrometer, peptides with m/z values less than 1250 Da were selected. Also, doubly or triply charged precursor ions were preferentially chosen since the ions were stable and reproducible for MRM quantitation. Most peptides containing prolines at P2 (xxxxPK/R) or P3 (xxxxPxK/R) sites were excluded from the lists because their prominent fragment ions (y_2 or y_3) might overlap with highly intense noise peaks between 300 and 400 Da, and these ions would be hard to distinguish from the interferences. However, we were able to select 7.1% out of the 281 peptides that were free from background interference. The peptides represent 147 TFs selected from 1191 lung cancer-related proteins (Figure 1).

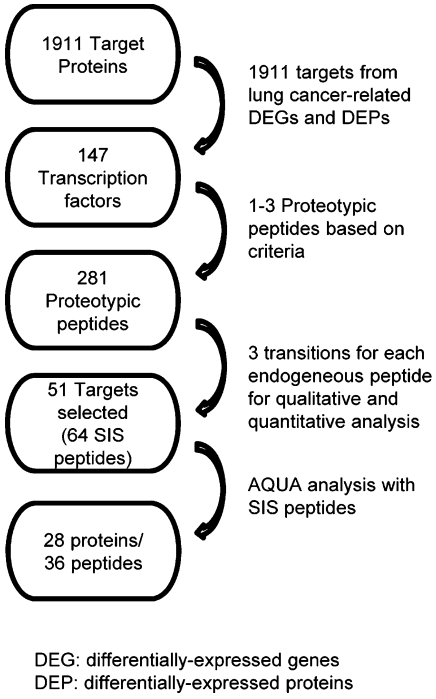

Figure 1. Overall experimental workflow for the TF MRM assay. The 1911 lung cancer-related proteins were collected after identifying DEGs and DEPs from previously reported somatic mutations, CGHs, epigenetic, gene expression, and protein profiles.

Other points of consideration were the specificity of tryptic digestion and unavoidable chemical modification during sample preparation. Peptides with basic amino acids (K or R) at P1′ site were excluded. In this case, the cleavage between two basic residues (such as KR, RK, RR, and KK) is often incomplete since it competes with the cleavage after the second residue. Prolines (P) after the tryptic site were removed for the same reason. Peptides with N-terminal glutamines (Q) were eliminated due to potential deamidation of the amide-containing side chains.[30] Peptides containing methionines (M) or cysteines (C) were removed because of their susceptibility to oxidation.

After refining the peptide lists on the basis of the aforementioned criteria, a BLAST search was performed to

dx.doi.org/10.1021/pr3011414 | J. Proteome Res. 2013, 12, 2582−2596

Table 1. Cell Lines Selected for MRM Experiments

name	disease	source	species	Google Scholar[a]	Pubmed[a]	metastatic site
A549	carcinoma	lung	human	48800	6342	x
Calu-1	carcinoma, epidermoid	lung	human	1460	113	pleura
NCI-H23	adenocarcinoma, NSCLC	lung	human	1210	55	x
NCI-H460	carcinoma, large cell	lung	human	3820	308	pleural effusion
NCI-H520	carcinoma, squamous cell	lung	human	384	33	x
NCI-H1299	carcinoma, large cell neuroendocrine	lung	human	620	81	lymph node
NCI-H69	carcinoma, small cell lung cancer	lung	human	1410	158	pleural effusion
H69AR	carcinoma, small cell lung cancer, multidrug resistant	lung	human	526	40	x

[a]The total number of citations for each cell line in Google Scholar and Pubmed at the time of data collection.

find unique peptides within the human genome. Three hundred ninety-five unique peptides representing 147 TFs were found using this procedure. Some proteins had more than 5 proteotypic peptides and others had only 1−3 peptides. Finally, priority was given to frequently observed peptides in MS databanks, GPM (19.9% of total peptides used in this experiment) and PeptideAtlas (8.5%). Most of the time, selected 3 peptides were used for a target TF, resulting in 282 proteotypic peptides for the initial MRM assay.

Synthetic Peptides

Crude peptides (282 peptides; SpikeTides, JPT Peptide Technologies) were purchased for experimental optimization of MRM transition parameters. Approximately 50 nmol of each peptide was provided by the vendor. The peptides were resolubilized in 200 μL of 20% acetonitrile (≥98%, J.T. Baker, NJ) with 1% formic acid (≥98%, Merck, Darmstadt, Germany) to make ∼250 nmol/mL stock solution. Subsequently, two dilution series (250 pmol/mL and 5 pmol/mL) of each stock solution were prepared. One out of the 282 peptides, LLEQSEWQPTNVDGK (IRF1), was not analyzed further because of incorrect synthesis, resulting in 281 peptides that were used for the rest of analysis.

For accurate quantification, stable isotope standard (SIS) peptides with C-terminal [$^{13}C_6$, $^{15}N_2$] lysine and [$^{13}C_6$, $^{15}N_4$] arginine (SpikeTides TQL, JPT Peptide Technologies), were purchased. The SIS peptides contained JPT tryptic tags and needed to undergo tryptic digestion to release the respective proteotypic peptides. For each sequence, amino acid analysis (AAA) was performed, and the absolute peptide amount was given by the vendor. All SIS peptides were spiked into cell line lysates prior to tryptic digestion.

Sample Preparation

Eight lung cancer cell lines, A549 (carcinoma), H460 (carcinoma; large cell lung cancer), H1299 (carcinoma; non-small-cell lung cancer), H23 (adenocarcinoma; non-small-cell lung cancer), Calu-1 (epidermoid carcinoma), H520 (squamous cell carcinoma), H69 (carcinoma; small cell lung cancer), and H69AR, were obtained from the American Type Culture Collection (Table 1). At the time of information collection for the cell lines, they were highly cited in the literature, on the basis of searches in done in Google Scholar and PubMed. The cells were cultured in RPMI1640 (Gibco, Rockville, MD) supplemented with 10% fetal bovine serum (Gibco, Rockville, MD), 1% penicillin and 1% streptomycin (Gibco, Rockville, MD) at 37 °C in a humidified 95% air, 5% CO_2 incubator. The cells were grown to approximately 70% confluency (approximately 7.0×10^6 cells) in 100 mm culture dishes (Nunc, Naperville, IL). After the cell monolayer was rinsed carefully with chilled phosphate buffered saline (PBS) 3 times, the intact cellular proteins were isolated. The PBS was removed by aspiration, and 500 μL of chilled lysis buffer (8 M Urea, 75 mM NaCl, 50 mM Tris pH 8.3) was used. The lysates were transferred into 1.5 mL tubes and sonicated three times with a 1 s pulse, with intermittent cooling for 19 s at 4 °C, and centrifuged at 12 000 rpm for 10 min at 4 °C to eliminate cell debris. Clear supernatants were collected in 1.5 mL Eppendorf tubes, and the amount of total proteins in the cells was measured by Bradford assay (Bio-Rad, Richmond, CA). The samples were stored at −80 °C when not in use.

To reduce disulfide bonds, 50 mM tris(2-carboxyethyl)-phosphine (TCEP) was added into 250 μg of the proteins to make final concentration at 5 mM, and the mixture was incubated with gentle shaking at 37 °C for 40 min. The reduced proteins were cooled down to room temperature (25 °C), and 140 mM IAA (iodoacetamide, alkylating reagent) was added to make the final concentration at 14 mM. The samples were diluted 10-fold with 50 mM Tris-HCl (pH 8.3), to dilute urea in the sample to less than 1 M. The synthetic crude peptides or the SIS peptides, if required, were spiked into the samples at this step. For the tryptic digestion, 100 mM $CaCl_2$ was added to make the final concentration 1 mM, and 1/100 (enzyme/substrate) trypsin was incubated with the samples at 37 °C for 16 h. To stop the reaction, 0.1% TFA (pH < 3.0) was added. Finally, samples were desalted with Sep-pak reversed phase cartridges (Waters, Milford, MA), dried via vacuum centrifugation, and stored at −20 °C until use.[31]

LC−MRM Setup

For optimization of MRM transitions, 7 to 8 synthetic peptides (5 pmol/mL stock solution) were mixed to prepare 40 different mixtures, which included 281 crude peptides, and each mixture was directly infused into a QTrap5500 hybrid linear ion-trap triple quadrupole mass spectrometer (ABSciex, Foster City, CA), equipped with TurboSpray source. MRM transitions for a total of 281 peptides were optimized.

MRM quantitation was performed on the mass spectrometer equipped with a nanoelectrospray ion source. Chromatographic separation of the peptides was performed using an Eksigent nanoLC-Ultra 1D plus (Eksigent Technologies, CA). Each sample was injected with a full sample loop injection of 1 μL and 1000 nL timed injection using mobile phase A (98% water, 2% acetonitrile, 0.1% formic acid). The protein concentrations of each sample were 2 μg/μL. Samples were separated on a column (75 μm × 12 cm) packed in house with Magic C18 (pore size 200 Å, particle size 5 μm) reversed-phase resin (Michrom Bioresources, Auburn, CA). A guard column (75 μm × 1 cm) was also used in order to protect the analytical column. A linear gradient of 2−30% mobile phase B (99.9% acetonitrile, 0.1% formic acid) for 40 min with a flow rate of 300 nL/min

dx.doi.org/10.1021/pr3011414 | J. Proteome Res. 2013, 12, 2582−2596

was applied for the separation, and elution at 80% mobile phase B for additional 10 min was used to wash the column followed by a 20-min re-equilibration time.

The MS was operated in the positive ion mode with the following parameters: ion spray voltage of 2100 V, curtain gas at 20 psi, nebulizer gas at 25 psi, resolution at 0.7 Da (unit resolution) for Q1/Q3, interface temperature at 150 °C, and scan mass range of 300−1250 m/z. The CE, collisional cell exit potential (CXP), and DP were set on the basis of the optimization results for the crude peptides. The identical experimental conditions were used for SIS peptides. Quantification experiments were performed using the scheduled MRM mode with an MRM detection window of 420 s and cycle time of 1.5 s. Figure S1 (Supporting Information) shows the optimized CE. Linear regression of the optimized CE was CE = 0.046 m/z − 0.621 V (R^2 = 0.754) for doubly charged precursors, and CE = 0.040 m/z + 0.780 V (R^2 = 0.489) for triply charged precursors.

Qualitative and Quantitative MRM Assays

For identification of targets in LC−MRM, a dilution series of the crude peptides was spiked into cell lysates and analyzed. Analyst software (version 1.5.1, Applied Biosystems/MDS Sciex) and MultiQuant software (version 1.2 Applied Biosystems/MDS Sciex, Foster City, CA) were used to interpret the data. The retention times and order of transitions obtained from the synthetic peptides were used to assign the target peptides from the endogenous TFs. Of the 281 peptides tested, 63 peptides were successfully assigned as detectable MRM targets, and their SIS peptides for quantitative analysis were purchased.

The previously measured average retention time of each peptide was used to set up the scheduled MRM analysis. Triplicate MRM runs for each cell line were performed to determine the repeatability of the experiment. The most intense transition of the 3 selected transitions was used to calculate the concentration of a peptide of a target TF. Peak areas were integrated by setting a 3-point Gaussian smooth width, a 30 s t_R half window, and a 2-point peak splitting factor in MultiQuant integration algorithm. The concentration of each peptide was determined by calculating the peak area ratio of endogenous peptide and the corresponding SIS peptide. The values were corrected by multiplying the slope of the peptide response curve. The final concentrations were averaged from triplicate MRM runs for each target.

To generate peptide response curves of the 63 peptides, a dilution series, 6−13 calibration points, of SIS peptides were spiked into a pooled sample matrix, and triplicate MRM experiments were performed for each dilution (reverse response curve). Peak areas of different concentration of SIS peptides were normalized to those of constant endogeneous peptides from the sample matrix. Standard curves were generated by linear regression of normalized peak areas as a function of SIS concentrations. The curves were used to predict the amounts of the endogenous peptides and to measure the lowest limit of quantitation (LLOQ), in which LLOQ was the lowest concentration of SIS peptides on the linear regression line within coefficient of variation (CV) ≤ 20% and coefficient of determination (R^2) ≥ 0.99. For the 35 peptides whose endogenous levels were below the LLOQs determined from a pooled cell lysate, the peak areas of SIS peptides were directly used without normalization.

Correlation Analysis between Protein and mRNA Abundances

To identify the relationships between MRM measurements and gene expression data of TFs in the six lung cancer cell lines (A549, H460, H1299, H23, Calu-1, and H520), we used the gene expression data sets (accession number = GSE8332[32]) obtained from Gene Expression Omnibus (GEO) database, a public genomics data repository.[33] To identify linear relationships, the gene expression data were linearly fitted with MRM measurements. On the other hand, to identify a nonlinear relationship, the gene expression data were fitted with log-transformed MRM measurements. The R^2 statistic, F statistic, and p-value for the fitted models were calculated as described in Walpole.[34] The fittings with p-values < 0.1 were identified as significant relationships.

Identification of DOX Resistance-Related TFs and Genes

To identify DOX resistance-related TFs, we quantified the levels of endogenous peptides using the corresponding SIS peptides. Using these data, we then identified 14 DOX-resistance related TFs as differentially expressed TFs (DETFs) between DOX-sensitive (H69) and -resistant cells (H69AR) with p-values < 0.05 from two-tailed t test and fold-change larger and less than 1.5. We further analyzed gene expression profiles (GEO data set accession number = GSE10841) generated from DOX-sensitive (H69) and -resistant cells (H69AR)[35] to identify DOX resistance-related genes. We first normalized the raw intensities using the GCRMA method (version 2.24.1 with R)[36] and then identified differentially expressed genes (DEGs) between H69 and H69AR cells with adjusted p-values ≤0.05 and log2-fold-changes ≥1.6 (3-fold), the 2.5th percentile (i.e., level of significance = 0.05 in the two-tailed test) of the null hypothesis distribution of the fold change estimated by performing the random permutation experiments as previously described.[37] To correlate DETFs with DEGs, we calculated the significance of the number of DEGs regulated by DETFs. The genes targeted by the 14 DETFs were first obtained from MetaCore (ver 6.7)[38] using the "expand by one interaction" algorithm with the following options: direction = "downstream" and interaction type = "transcription regulation". Only manually curated high-confidence TF−target interactions were used. Using the TF−target interactions, we then identified the target DEGs regulated by the 14 DETFs. Finally, we computed the significance of the number of target DEGs as follows: (1) we randomly selected the same number of genes from all the genes spotted on the same microarray as that of the upregulated (or downregulated) genes; (2) we then identified the number of target genes regulated by the 14 DETFs; (3) we repeated steps 1 and 2 100 000 times and then estimated an empirical distribution of the number of target genes of the 14 DEFTs; and (4) we computed a p-value as the area under the empirical distribution from the observed number of up-regulated (or down-regulated) target genes of the 14 DETFs in the data to more extreme than the observed number.

Identification of Cellular Processes Represented by the DEGs and Network Analysis

We identified gene ontology biological processes (GOBPs) represented by the following sets of genes using DAVID software:[39] DEGs between H69 and H69AR and a subset of DEGs regulated by the 14 DETFs. GOBPs assigned to each gene by the gene ontology consortium imply cellular processes in which the gene is involved.[40] For each set of genes, we identified the GOBPs represented by the genes with P < 0.05.

dx.doi.org/10.1021/pr3011414 | J. Proteome Res. 2013, 12, 2582−2596

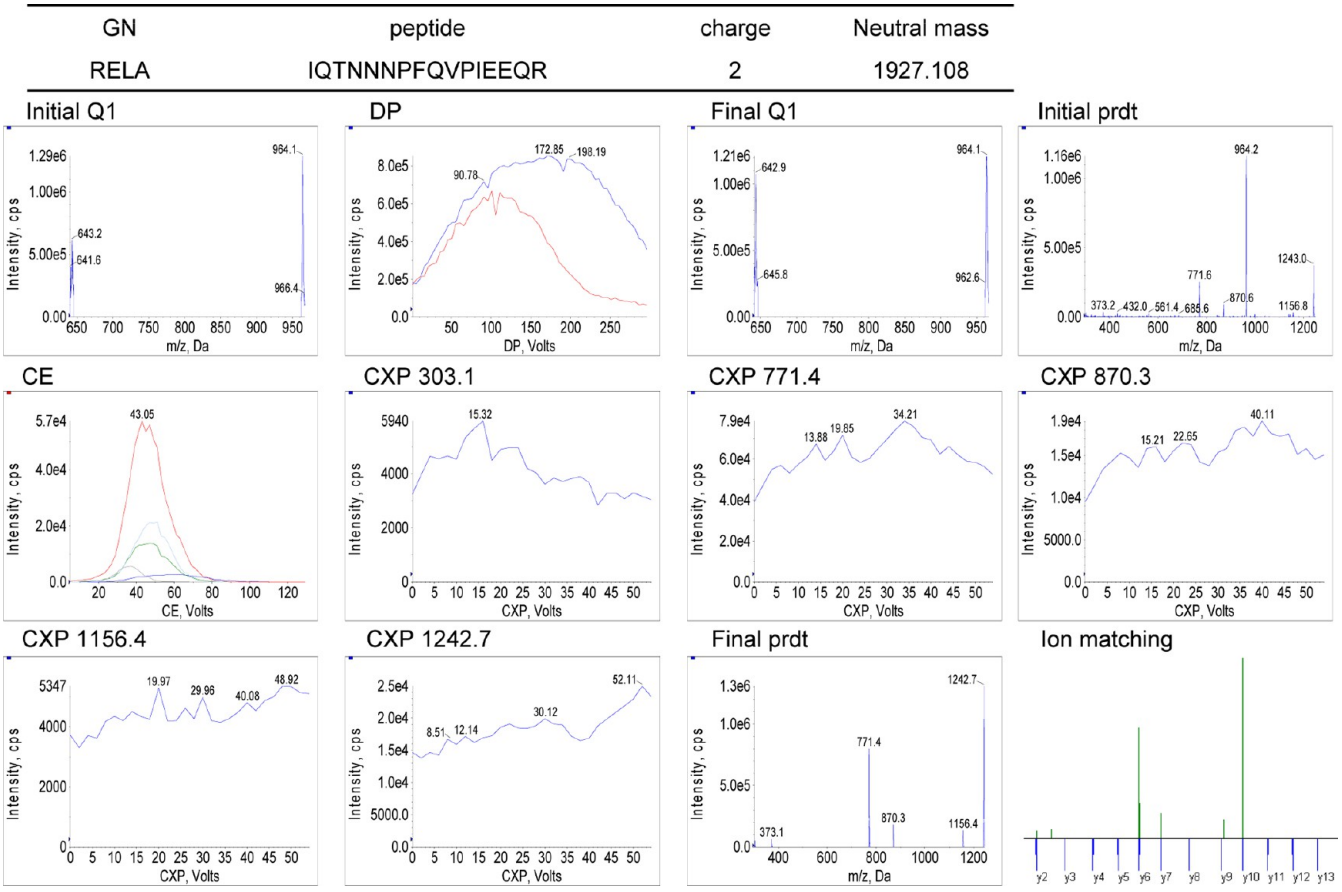

Figure 2. Optimization of a representative proteotypic peptide of v-relreticuloendotheliosis viral oncogene homologue A. Initial Q1 scans for doubly and triply charged ion were performed with the instrumental default DP setting (180 V), and the optimized DP for doubly (blue) and triply (red) charged ions was found by ramping the voltage. The initial product ion scan for the dominant charge state, doubly charged ion, was performed with the optimized DP, and 10 most intense product ions were selected for CE optimization. CXP was also optimized for the 5 most intense transitions. As a final step, the product ions were scanned using all of the optimized instrumental parameters, and the spectra were matched with the theoretical MS fragmentation pattern. Experimental procedure followed was as shown in Figure S1 (Supporting Information).

Among the GOBPs, we selected the GOBPs commonly represented by both DEGs and targets of the 14 DETFs. Finally, we generated a transcriptional regulatory network using the 14 TFs and their targets involved in the selected GOBPs. The network was visualized using Cytoscape (v. 2.8.1).[41] The nodes with the same GOBPs were grouped into the same modules, each of which was named by the corresponding GOBP.

RESULTS

Identification of Lung Cancer-Related TFs by Integrating Genomic and Proteomic Data

We first collected previously reported somatic mutations,[42−46] CGHs,[42,47−49] and epigenetic data[50−53] associated with lung cancer. We also obtained gene expression[54−59] and proteome profiles[60−65] generated from lung cancer patients or cell lines. Using these gene expression profiles, we identified DEGs between lung cancer and healthy tissues using a previously reported method.[37] We also collected data on differentially expressed proteins (DEPs) in lung cancer tissues or cells from six previous studies.[60−65] Among these DEGs and DEPs, we defined lung cancer-related genes and proteins as the ones that were detected more than twice. By combining all of these lung cancer-related signatures, we were able to identify 1911 factors that indicated the presence of lung cancer by at least one of these signatures (Figure 1). From these 1911 factors, we finally identified 147 lung cancer-related TFs as the ones with transcriptional factor or regulator activity according to their GO molecular functions (GOMFs, Table S1, Supporting Information). GOMFs assigned to each gene by the gene ontology consortium imply functions (e.g., kinase activity or DNA binding) that the gene has.[40]

Assigning Peptide Peaks of Endogenous TFs on MRM Chromatogram

We selected 281 peptides for the 147 TFs and purchased their crude synthetic peptides followed by optimizing MRM transitions (Figure 1). Once the MRM transitions were optimized (Figure 2, Figure S2, Supporting Information), we located the MRM chromatographic peaks for the endogenous peptides during the LC runs. First, we applied daughter ion scan mode in QTrap5500 to the A549 crude extract. In this mode, the enhanced product ion (EPI) scan of the linear ion trap (LIT) was used instead of Q3, the third quadrupole. Representative data are shown for a proteotypic peptide, LPVDLAEELGHR from CDKN2A, in Figure 3A. The ion intensities were too low to be identified with commercially available search engines such as MASCOT, SEQUEST, etc (bottom spectrum). Even with nearly 20 fmol of synthetic peptide, peak assignment was impossible from the EPI daughter ion scan (middle spectrum of Figure 3A). Instead, a dilution

dx.doi.org/10.1021/pr3011414 | J. Proteome Res. 2013, 12, 2582−2596

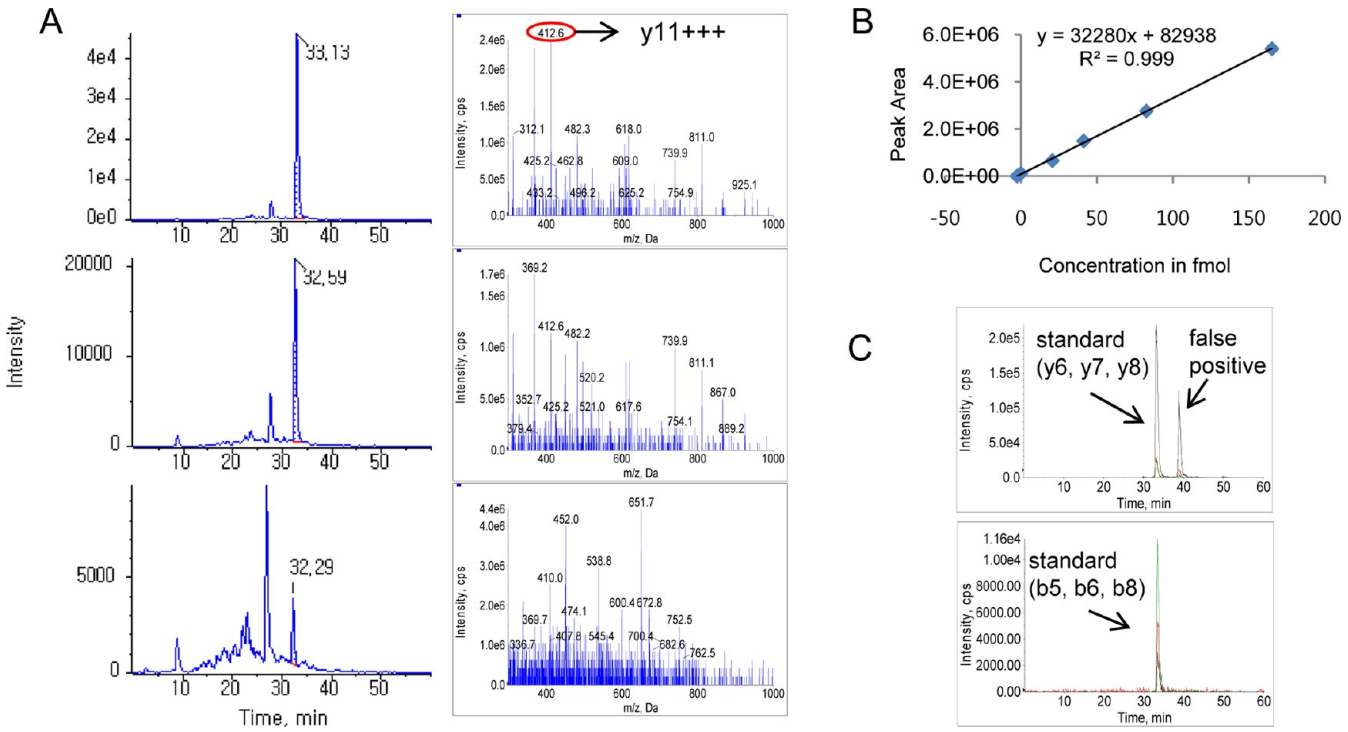

Figure 3. Assigning an MRM chromatogram. (A) Comparison of EPI scan of LIT (right) and MRM measurement (left) with identical sample concentration; 0, ~20 and ~40 fmol of a crude peptide (LPVDLAEELGHR) from CDKN2A. Of the three selected transitions, the most intense ion, y11+++, was used for generating the MRM chromatogram. (B) Rough estimation of the endogenous peptide concentration by standard addition method, with five dilutions of a crude peptide solution. (C) Peak assigning in the case of impurities (RELA, IQTNNNPFQVPIEEQR). To clarify the ambiguous chromatogram, a combination of various transitions was used.

series of the crude synthetic peptide for an endogenous peptide was spiked into A549 cell extract, and three y-ions, y11+++, y3+ and y11++, were monitored using the transition parameters optimized by direct infusion. Without the spiked-in peptide standard, there were many peaks, and noise peaks were present (bottom chromatogram of Figure 3A), among which only the peak at retention time 32.3 min was able to be identified as genuine since it showed increased intensity in the presence of spiked peptide (top and middle chromatograms of Figure 3A). In addition, peak areas showed a linear correlation with the amount of added synthetic peptide as shown in Figure 3B, from which a rough estimation of the endogenous level of LPVDLAEELGHR peptide could be made.

In some cases, crude synthetic peptides showed more than one chromatographic peaks, as is exemplified by the IQTNNNPFQVPIEEQR peptide from RELA in Figure 3C. Two peaks at different retention times were observed when three y-ions, y6, y7 and y10, of the peptide were used. To identify the real standard peak, we also monitored b-ions, b5, b6 and b8, and found that the earlier-eluting peak represented our peptide, while the later peak was a false positive. It may have originated from impurities, presumably from synthetic byproducts sharing the same C-terminal region but with a different N-terminal region than the correct peptide.

All assignment processes were performed prior to quantification. After excluding the peptides that were not detected in any of the cell lines, we finally assigned MRM peaks for 36 peptides representing 28 endogenous TFs and purchased their SIS peptides for quantitative analysis.

Linear Response and LLOQ of SIS Peptide in Sample Matrix

Calibration curves were generated with a dilution series of spiked SIS peptides in a pooled sample matrix (Figure 4 and Figure S3, Supporting Information). Triplicate MRM measurements were performed for each concentration, and a highly intense transition of a peptide was used to construct the curves. To determine limit of quantification (LOQ), conventional LOQ estimation, such as signal-to-noise, blank determination, and linear regression, was applied. However, in this particular study, we also determined the LLOQ for practical MRM quantitation since the filtering system in quadrupole effectively eliminates most undefined transitions during analysis,[18,66] and the stabilized ionization of the blank in MS might produce low standard deviation for baseline signal, resulting in lowering the LOQ. In fact, the instrumental response to high backgroud makes the chromatographic baseline unstable, resulting in high CVs at low concentrations of analytes. Therefore, we defined the practical LLOQ to be a CV $\leq$ 20% and $R^2 \geq 0.99$ as shown in Figure 4A. Using this definition, the LLOQs of CBL and PURA were 293 and 195 amol, respectively (see also Table S2, Supporting Information). Of the 36 peptides determined, the minimum LLOQ was 15 amol and the maximum was 1.9 fmol (Figure 4B).

The calibration curves were used to predict the approximate concentrations of the SIS peptides for quantitative analysis, where the concentration of SIS peptide added to each cell lysate was based on the standard curve. Once the concentration of an endogenous peptide was measured, it was multiplied by the analytical response factor (i.e., the slope of the curve), to correct the concentration.

dx.doi.org/10.1021/pr3011414 | J. Proteome Res. 2013, 12, 2582−2596

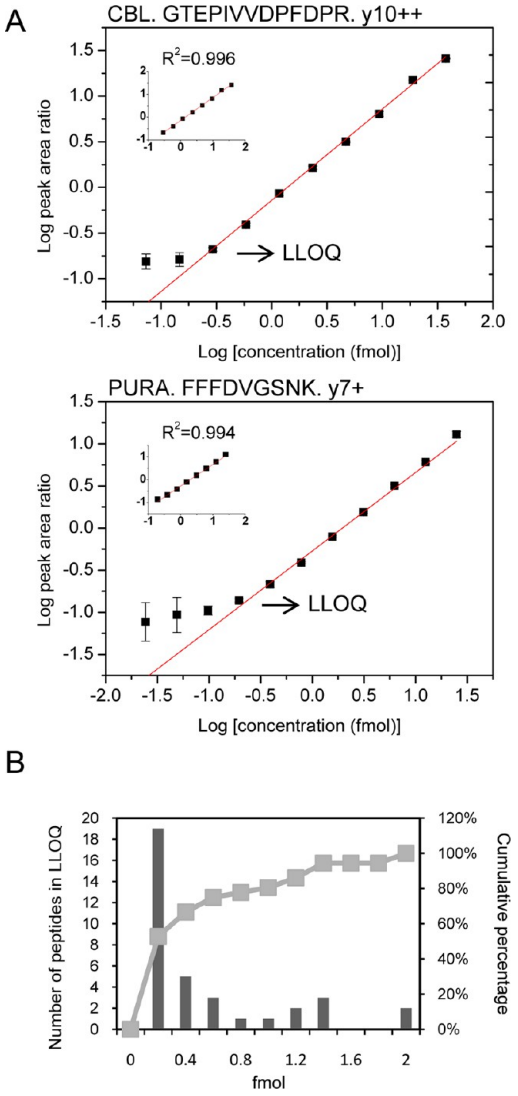

Figure 4. Representative calibration curves. (A) A dilution series of the SIS peptides for CBL GTEPIVVDPFDPR (y10++), and PURA FFFDVGSNK (y7+) were spiked into a pooled sample matrix. Insets show the linear range of the curves with $R^2 \geq 0.99$ and CV $\leq$ 20% to determine the LLOQ. (B) Cumulative analysis of the LLOQs for 36 peptides.

Quantification of TFs in Whole Cell Lysates

We quantified 36 peptides representing 28 endogenous TFs in 8 lung cancer-related cell lines. Out of 288 MRM measurements (36 peptides × 8 cell lines), 241 were successfully quantitated (Figure 5, Table 2, and Figure S5, Table S2, Supporting Information). The measurements showed an average CV of 9.7%, a median CV of 7.4%, and a minimum CV of 0.2%. The minimum concentration was 15.1 amol/μg with a CV of 69.5% (cell line: A549, gene name: KLF4, peptide sequence: TTPTLGLEEVLSSR), and the maximum concentration was 311.96 fmol/μg with a CV of 0.9% (H69AR, ENO1, YISPDQLADLYK). The minimum concentration with CV $\leq$ 20% was 19.4 amol/μg with a CV of 6.3% (A549, STAT2, EVLQSLPLTEIIR). Of 241 MRM measurements, 221 (91.7%) showed CVs of $\leq$20%, 149 (61.8%) had CVs of $\leq$10%, and 96 (39.8%) had CVs of $\leq$5%.

The amounts of target TFs varied depending on the type of cell lines and the susceptibility to DOX. CDKN2A (LPVDLAEELGHR) could be quantified only in H69 and H69AR cell lines, while EGR2 (SLDLPYPSSFAPVSAPR) could not be quantified in these cell lines (Figure S5, Supporting Information). In case of CSDA, the concentration could be determined in the DOX-resistant cell line H69AR but not in H69 (Figure 6). The peak for the endogenous peptide (GAEAANVTGPDGVPVEGSR, red trace in Figure 8) in H69AR was clearly detected and estimated to be 1.9 fmol/μg, but the peak for this peptide in H69 was very low, close to the sample noise level. We also found that the detection of CTNNB1 was also cell-dependent. In H520 cells, the amount of CTNNB1 (LLNDEDQVVVNK) was characteristically higher (21.2 fmol/μg) than the other cell lines (1.7 to 3.6 fmol/μg). This characteristic was clearly shown with the other peptides of CTNNB1, although the numerical values were slightly different between peptides (Figure 5).

For the quantitation of the target proteins, we used one to three proteotypic peptides of a TF. A highly intense transition of each peptide was used to accurately quantify the individual proteotypic peptides. For ENO1, KLF4, PURA, RELA, and SMAD4, which were quantified on the basis of two or three peptides, the protein concentrations varied depending on the peptide used for measurement, as did that of CTNNB1. However, the concentration difference for a selected peptide between cell lines was similar. For example, three peptides of CTNNB1 and two peptides of ENO1 showed similar concentration differences in each cell line (Figure S5, Supporting Information).

Correlation between Protein and mRNA Abundances in Lung Cancer Cells

MRM measurements were compared with the gene expression data of TFs in the six lung cancer cell lines (A549, H460, H1299, H23, Calu-1 and H520) obtained from the gene expression data set (accession number = GSE8332[32] in GEO database). Among the 22 peptides from 16 proteins quantified in all six cell lines, FGGNPGGFGNQGGFGNSR from TARDBP showed a linear relationship between protein and transcript abundances (Figure 7A) while SSQPLASK from HMGA1 showed a nonlinear relationship (Figure 7B). However, most of the peptides showed no significant correlation with their mRNA levels, as has been previously described for other higher organisms.[67] On the basis of the correlation, these peptides can be categorized into the following two groups: (1) seven proteins (SMAD4, PTTG1, SMAD4, LZTR1, SMAD4, STAT2, and STAT1) for which seven peptides and their mRNAs were both detected, showed no significant correlation between the levels of mRNAs and proteins (a representative peptide, EVLQSLPLTEIIR from STAT2, is shown in Figure 7C); and (2) 10 proteins (RELA, CTNNB1, EGR2, CSDA, ENO1, FOXO3, CBL, PAX5, PURA, and STAT3) for which 15 peptides were detected while mRNAs were not detected, thereby showing no correlation (a representative peptide, YISPDQLADLYK from ENO1, is shown in Figure 7D). These results highlight the sensitivity of the MRM assays. The protein-per-mRNA ratios are different for individual genes and also vary under different conditions. Thus, the discrepancy between mRNA and protein abundances further indicates that the precise abundances of TFs measured using multiplexed MRM assays is useful for understanding their functions, as described below.

dx.doi.org/10.1021/pr3011414 | J. Proteome Res. 2013, 12, 2582−2596

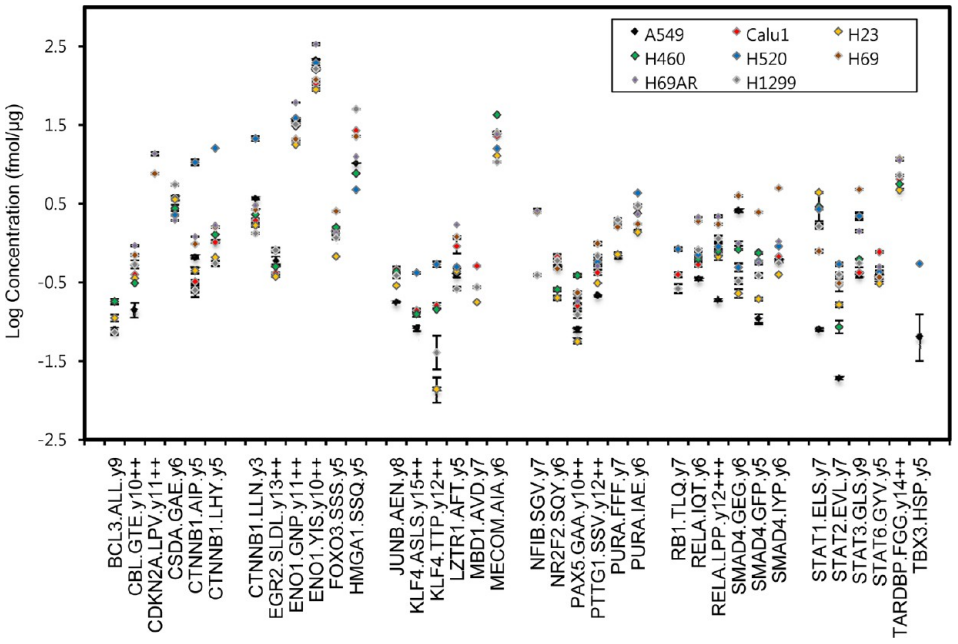

Figure 5. Quantitative analysis of 241 proteotypic peptides in 8 cell lines. Optimized instrumental parameters for the most intense three transitions of the peptides were used for the SIS peptides. A scheduled MRM algorism was used for simultaneous MRM measurement of 36 peptides in a single run. The most intense transitions for peptides were used to determine the concentrations. The average concentrations of triplicate MRM measurements for individual target are shown with standard error bars. The concentrations for each of the 8 cell lines are presented separately in Figure S5 (Supporting Information).

TFs Related to DOX Resistance in Lung Cancer Cells

The MRM assays were used to measure the abundances of TFs in order to investigate DOX resistance in small cell lung cancer (SCLC). Using the MRM assays, 28 peptides from 21 proteins were quantified in DOX-sensitive (H69) and -resistant cells (H69AR) before and at three different times (1, 6, and 8 h) after DOX treatment. In these experiments, we identified 18 peptides from 14 differentially expressed TFs (DETFs; $P < 0.05$). Nine (12 peptides) of 14 DETFs were differentially expressed at basal level ($T = 0$), while the other five DETFs were differentially expressed at least once at $T \geq 1$ (Table S4 and Figure S7, Supporting Information). Group 1 contained STAT1, ENO1, CSDA, and CDKN2A, which were up-regulated in H69AR at $T = 0$. Group 2 contained SMAD4, FOXO3, STAT3, HMGA1, and PTTG1, which were down-regulated at $T = 0$. Group 3 contained CBL, LZTR1, and STAT6, which were up-regulated at $T \geq 1$. Group 4 contained CTNNB1 and RELA, which were down-regulated at $T \geq 1$. Interestingly, many of the 14 DETFs have been previously reported to be associated with resistance of various drugs, including DOX (Table S5, Supporting Information). Specifically, STAT1[68,69] and SMAD4[70] were associated with resistance to DOX. These different expression patterns over time in the four groups of 14 DETFs indicate that they are involved in distinct pathways defining DOX resistance in SCLC.

Potential Association of the DETFs with DOX Resistance in SCLC

To investigate the possible association of the 14 DETFs with DOX resistance, we first identified 2144 DEGs between H69 and H69AR SCLC cells, 1022 up-regulated and 1124 down-regulated genes in H69AR cells (Table S6, Supporting Information). We then examined how many of the DEGs could be regulated by the 14 DETFs. According to TF−target information in MetaCore, 211 (21%; $P < 10^{-5}$) of the 1022 up-regulated genes and 212 (19%; $P < 10^{-5}$) of the 1124 down-regulated genes in H69AR are targets of the 14 DETFs (Figure 8A; Table S6, Supporting Information). Next, we examined which cellular processes associated with DOX resistance can be regulated by the 14 DETFs. We first identified DOX resistance-related cellular processes as the GOBPs represented ($P < 0.05$) by 1022 up-regulated and 1124 down-regulated genes in H69AR. Interestingly, many of these DOX resistance-related GOBPs were also represented by 423 targets of the 14 DETFs (Figure 8B; Table S7, Supporting Information), including drug-resistance related signaling pathways (MAPKKK, JAK-STAT, Wnt, and TGF-beta signaling pathways; Table S5, Supporting Information). We then examined which TFs regulate these GOBPs by counting how many of the genes involved in the GOBPs are regulated by the DETFs. Among the DETFs, RELA in the MAPKKK cascade, STAT1, 3, 6 in the JAK-STAT cascade, and CTNNB1 and SMAD4 in the TGF-beta signaling pathway are the major regulators of the genes associated with DOX resistance (Figure 8C). We then generated a network model that delineates the relationships of the major DETFs and their targets involved in the GOBPs (Figure 8D). The dense interactions among the genes involved in the GOBPs indicate that the major DETFs collectively regulate DOX resistance-related cellular processes. Therefore, the results support the utility of the proposed multiplexed MRM assays.

DISCUSSION

Lung cancer-related TFs were quantified by MRM without prior affinity depletion or subfractionation of cell lysates. Since they are largely present in low abundance, we carefully designed experimental procedures including selection of Q1 and Q3 and optimization of MRM transitions. Special consideration was made for the selection of the m/z values of the product ions. We first investigated peptides with prolines positioned at P2 and P3 since some of these ions had highly sensitive MRM

dx.doi.org/10.1021/pr3011414 | J. Proteome Res. 2013, 12, 2582−2596

Table 2. Experimental MRM Conditions for 36 Quantified Proteotypic Peptides Representing 28 Transcription Factors[g]

		light[a]		heavy[b]		charge state						
gene name	peptide sequence	Q1	Q3	Q1	Q3	Q1	Q3	ion	DP[c]	CE[d]	CXP[e]	avg t_R[f]
BCL3	ALLDSAAPGTLDLEAR	807.187	971.400	812.191	981.409	2	1	y9	151	35	44	36.45
CBL	GTEPIVVDPFDPR	721.591	578.000	726.595	583.004	2	2	y10	146	25	28	38
CDKN2A	LPVDLAEELGHR	450.306	618.500	453.642	623.504	3	2	y11	101	19	28	34.48
CSDA	GAEAANVTGPDGVPVEGSR	891.960	644.400	896.964	654.409	2	1	y6	161	39	30	25.81
CTNNB1	LHYGLPVVVK	375.555	541.400	378.226	549.414	3	1	y5	76	13	24	32.04
	AIPELTK	386.332	587.400	390.339	595.414	2	1	y5	81	13	26	24.47
	LLNDEDQVVVNK	693.480	360.200	697.487	368.214	2	1	y3	86	29	18	26.31
EGR2	SLDLPYPSSFAPVSAPR	902.682	688.400	907.686	693.404	2	2	y13	131	33	32	40.43
ENO1	GNPTVEVDLFTSK	704.003	618.500	708.010	622.507	2	2	y11	166	27	28	35.63
	YISPDQLADLYK	713.584	575.400	717.591	579.407	2	2	y10	121	29	24	38.02
FOXO3	SSSFPYTTK	509.448	609.400	513.455	617.414	2	1	y5	76	23	28	23.78
HMGA1	SSQPLASK	409.222	515.400	413.229	523.414	2	1	y5	86	17	22	9.41
JUNB	AENAGLSSTAGLLR	680.651	804.500	685.655	814.509	2	1	y8	136	29	36	31.11
KLF4	TTPTLGLEEVLSSR	752.023	650.900	757.027	655.904	2	2	y12	106	31	30	40.06
	ASLSAPGSEYGSPSVISVSK	962.200	747.500	966.207	751.507	2	2	y15	146	41	36	31.76
LZTR1	AFTTGTPPAPR	558.370	537.400	563.374	547.409	2	1	y5	126	23	26	23.13
MBD1	AVDPGLPSVK	491.800	697.500	495.807	705.514	2	1	y7	96	21	30	26.61
MECOM	AIASIAEK	401.784	618.400	405.791	626.414	2	1	y6	91	15	28	20.41
NFIB	SGVFNVSELVR	603.952	816.500	608.956	826.509	2	1	y7	111	25	36	38.45
NR2F2	SQYPNQPTR	545.846	712.300	550.850	722.309	2	1	y6	106	25	34	16.58
PAX5	GAAPPAAATAYDR	616.416	516.800	621.420	521.804	2	2	y10	101	25	24	21.97
PTTG1	SSVPASDDAYPEIEK	804.541	668.000	808.548	672.007	2	2	y12	126	31	32	26.85
PURA	IAEVGAGGNK	458.243	503.300	462.250	511.314	2	1	y6	86	21	24	14.67
	FFFDVGSNK	530.629	766.400	534.636	774.414	2	1	y7	111	23	32	36.16
RB1	TLQTDSIDSFETQR	821.187	882.400	826.191	892.409	2	1	y7	146	37	38	30.85
RELA	LPPVLSHPIFDNR	502.709	465.100	506.045	468.436	3	3	y12	101	19	20	35.6
	IQTNNNPFQVPIEEQR	964.142	771.400	969.146	781.409	2	1	y6	171	43	34	34.51
SMAD4	GFPHVIYAR	353.972	621.500	357.308	631.509	3	1	y5	66	17	28	28.43
	GEGDVWVR	459.298	731.400	464.302	741.409	2	1	y6	101	19	34	25.28
	IYPSAYIK	477.850	678.500	481.857	686.514	2	1	y6	91	15	30	28.03
STAT1	ELSAVTFPDIIR	681.035	861.500	686.039	871.509	2	1	y7	121	29	34	41.42
STAT2	EVLQSLPLTEIIR	756.234	841.500	761.238	851.509	2	1	y7	171	31	42	43.88
STAT3	GLSIEQLTTLAEK	702.007	1032.400	706.014	1040.414	2	1	y9	131	29	48	40.52
STAT6	GYVPATIK	424.840	529.300	428.847	537.314	2	1	y5	86	15	24	24.48
TARDBP	FGGNPGGFGNQGGFGNSR	864.039	676.500	869.043	681.504	2	2	y14	111	39	35	29.16
TBX3	HSPATISSSTR	381.616	537.300	384.952	547.309	3	1	y5	61	17	24	14.7

[a]Light peptides represent endogenous peptides in cell lines. [b]Heavy peptides represent SIS peptides. [c]Declustering potential. [d]Collisional energy. [e]Collisional cell exit potential. [f]Average retention times were applied for scheduled MRM. [g]Experimental conditions for all 281 peptides can be found in the Supporting Information.

signals. In our study, 81 (28.8%) ions out of the 281 predominant ions showed the high peak intensities even though their m/z values were lower than the precursor m/z values; 17.1% were doubly or triply charged product ions, 3.2% were b-ions, 6.3% were ions produced by fragmentation at the N-terminal side of proline, and 2.1% were other y-ions (Supporting Information). For instance, GTEPIVVDPFDPR (precursor = m/z 721.6), a proteotypic peptide of CBL, showed relative ion intensities of y10++ (m/z 578.0) and y5 (m/z 631.3) of 100 and 69% compared to 62.8% for y7 (m/z 845.5), even though y7 had a higher m/z than the precursor ion. Also, the y5 (m/z 561.4) ion from AELAATLGLSER (precursor = m/z 616.0) of CDX2 showed nearly double the intensity of the y8 ion (m/z 846.5). In another case, the y3 from EGPGTPTR of ZBTB16 showed extremely high intensity compared to the other transitions.

Assigning tandem MS data, SEQUEST and MASCOT-like search engines can provide qualitative information in a shotgun approach. Likewise, qualitative analysis was possible with the LIT mode of the hybrid triple quadrupole. Also, by using peptide retention time prediction algorithms such as those in MaRiMba and Skyline, it was possible to identify a target peak even below 400 m/z even though the peak significantly overlapped with background noise. However, when the concentration of analytes was lowered, the identification was difficult and some selected transitions overlapped with noise peaks, generating a different transition ranking compared to the original transition peak rank order. In order to resolve this problem, various transitions were used for the identification, and transition peak rank order was investigated (Figure 3C). If multiple transitions were not available because of a single highly intense transition from a proline-containing peptide, the MRM data were confirmed by creating a dilution series of from the standard target peptide since only transitions from the target peptide should respond to the added standard (Figure 3).

dx.doi.org/10.1021/pr3011414 | J. Proteome Res. 2013, 12, 2582−2596

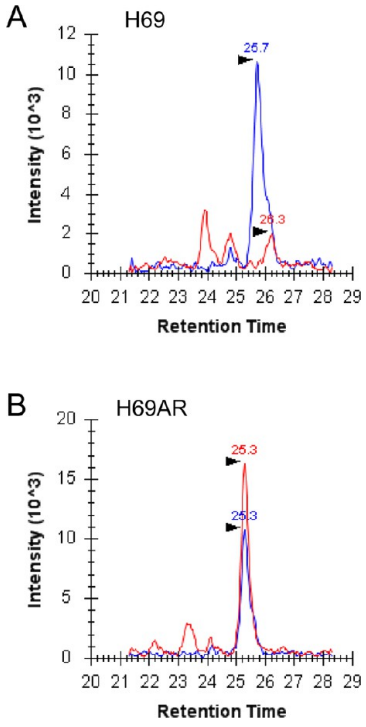

Figure 6. MRM analysis of CSDA (GAEAANVTGPDGVPVEGSR) in H69 (A) and H69AR (B). The y6 ions for the endogenous (red) and SIS peptides (blue) were monitored under identical experimental conditions.

We found it necessary to optimize the transitions and experimental parameters empirically.[14,18] Recently, many MRM softwares and web-based programs have become available, where all transitions and parameters can be collected from shotgun-based data or prediction algorithm. By using them, one should be able to simplify a MRM workflow and save a lot time. However, this approach might be limited to only high- and medium-abundance targets. For low-abundance targets, these parameters should be carefully optimized since optimal transitions and parameters might be slightly different from those given by the programs (see Figure S1 and Table S3, Supporting Information), and using the parameters from the programs could result in loss of instrumental sensitivity. Consistent with this conclusion, a recent report has shown that the MRM results applying the parameters are not identical for different models and instrument vendors.[20] We attribute our improved instrumental sensitivity to empirical optimization of our TF targets. The LLOQs are dependent on the nature of the selected peptides and the sample matrix used, and most of the LLOQs that we found for cell lysates were lower than those found previously published papers using plasma.[15,18] For plasma, Kuzyk et al. reported 0.015 fmol (7.5% CV) to 168 fmol (15% CV) within CV of 20%,[18] and Whiteaker et al. determined 0.2 fmol (6.6% CV) to 261.7 fmol (10.6% CV) by using the blank measurement method.[15] In this study on cell lysates, a simpler matrix, the LLOQs were between 0.065 and 1.9 fmol in a pooled sample. In A549, STAT2 could be quantified as low as 19.4 amol/μg with a CV of 6.3%. Usually,

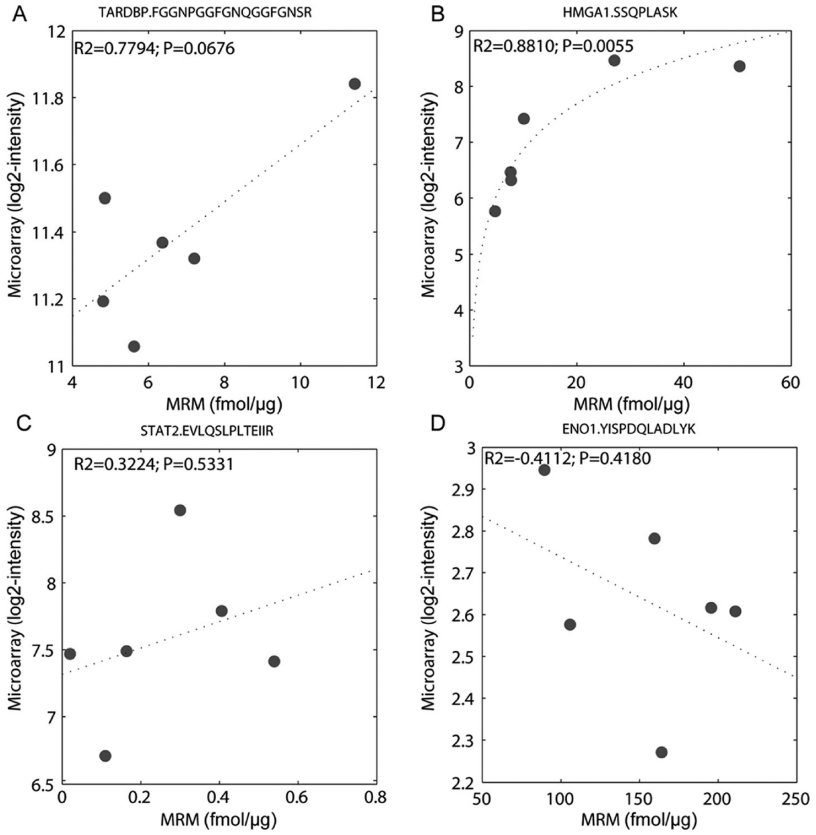

Figure 7. Correlation between protein and mRNA abundances in six SCLC cell lines. Quantification of four peptides and the expression levels of the corresponding genes were compared in scatter plots. In the scatter plots, the dotted line represents a linear (A, C, and D) and a logarithmic fit (B). R^2 and p-values denote goodness-of-fits.

dx.doi.org/10.1021/pr3011414 | J. Proteome Res. 2013, 12, 2582−2596

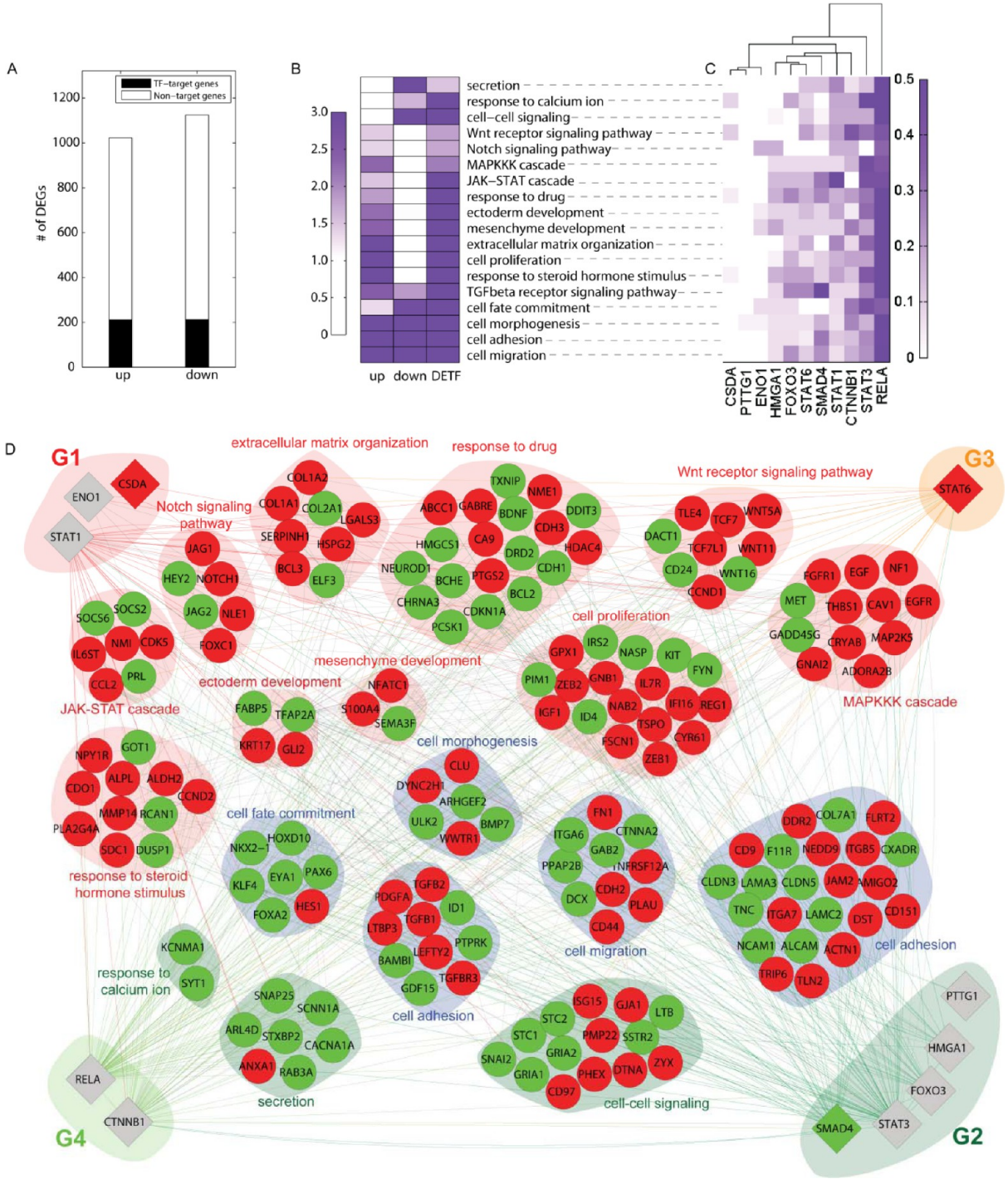

Figure 8. Potential associations of DETFs with DOX resistance. (A) The number of targets of the 14 DETFs among the DEGs (up- and down-regulated genes in H69AR cells, compared to H69 cells). (B) GOBPs represented by up- (up) and down-regulated genes (down) in H69AR and target DEGs of the 14 DETFs (DETF). Color bar, $\log_{10}$-P from the analysis for identification of GOBPs represented by the DEGs. (C) The number of targets of each DETF involved in the GOBPs. Color bar, the ratio of the number of targets of each DETF to the number of genes with the GOBP. (D) A network model showing the relationships between the DETFs and their targets. The nodes with same GOBPs were grouped into the same modules, each of which was named according to the corresponding GOBP. The red and green edges represent up-regulated TFs–target and down-regulated TFs–target interactions, respectively. Gray edges are protein–protein interactions between DETF targets. Red and green node colors represent up- and down-regulation of the genes in H69AR cells. Diamond and circle nodes denote DETF and their target genes of transcriptional regulation. Red, green, and blue background colors denote the GOBPs represented by (1) up-regulated genes in H69AR and targets of the DETFs, (2) down-regulated genes in H69AR and targets of the DETFs, and (3) up- and down-regulated genes as well as targets of DETFs, respectively.

STAT2 quantification in MS requires an additional enrichment step or fractionation step to concentrate the target.[71,72]

For TFs quantified with two or three peptides, protein concentrations varied depending on the peptide used for measurement. Theoretically, all the peptide concentrations should be identical and represent the concentration of the source protein in a sample. However, there seems to be an influence of enzymatic digestion efficiency during sample

dx.doi.org/10.1021/pr3011414 | J. Proteome Res. 2013, 12, 2582–2596

preparation or ionization effects in MS.[73−75] We also investigated, using a larger protein database, UniProt (version 2012_06), whether the peptides might represent different isoforms of a protein or contain known posttranslational modification sites or natural variations. Neither isoforms of a single protein nor known amino acid variations were found in the peptides for CTNNB1, KLF4, PURA, RELA and SMAD4. Thus, it seems that the observed differences in peptide levels are intrinsic to each protein. Nevertheless, the concentration difference of a specific selected peptide between cell lines was similar. Interestingly, the amount of the N-truncated isoform of ENO1 (GNPTVEVDLFTSK) was significantly different from the sequence YISPDQLADLYK, which was contained in both the truncated isoform and the natural form (Figures S5 and S6, Supporting Information). This difference is presumably due to differing amounts of the N-truncated form in the different cell lines.

The integrative analysis of MRM measurements and mRNA data confirmed the utility of the multiplexed MRM assays. This analysis provided a list of potential TFs that regulate the genes involved in drug resistance-related signaling pathways and cell differentiation processes, which are associated with DOX resistance in H69AR SCLC cells. Among these TFs, STAT1 and SMAD4 were previously reported to be closely involved in DOX resistance.[68,70] Moreover, many TFs and their targets involved in DOX resistance-related processes are linked to each other. These data collectively suggest that modulation of these TFs can control DOX resistance-related processes, which can be applied to identify a therapeutic option to treat SCLC patients showing DOX resistance. Specifically, the major downstream TFs (RELA, STAT1, 3, 6, CTNNB1, and SMAD4) of MAPK, JAK-STAT, and TGF-beta signaling pathways could be modulated to control DOX resistance in SCLC patients. Thus, mechanisms underlying the roles of the major TFs in DOX resistance can be the subject of detailed functional studies.

■ ASSOCIATED CONTENT

Supporting Information

Supporting tables, figures, and data. This material is available free of charge via the Internet at http://pubs.acs.org.

■ AUTHOR INFORMATION

Corresponding Author

*Phone: +82 2 958 6788. Fax: +82 2 958 5909. E-mail: clee270@kist.re.kr.

Notes

The authors declare no competing financial interest.

■ ACKNOWLEDGMENTS

This study was supported by the Proteogenomics Research Program funded by the Korean Ministry of Education, Science and Technology, Republic of Korea.

■ ABBREVIATIONS

AAA, amino acid analysis; CE, collisional energy; CV, coefficient of variation; CXP, collisional cell exit potential; DIA, data independent acquisition; DP, declustering potential; EPI, enhanced product ion; LIT, linear ion trap; LLOQ, lowest limit of quantitation; LOQ, limit of quantitation; MRM, multiple reaction monitoring; QQQ, triple quadrupole mass spectrometer; R^2, coefficient determination; SIS, stable isotope standard; TF, transcription factor; DEG, differentially expressed genes; DETF, differentially expressed transcription factor; DOX, doxorubicin; GOBP, gene ontology biological process

■ REFERENCES

(1) Yalow, R. S.; Berson, S. A. Immunoassay of endogenous plasma insulin in man. *J. Clin. Invest.* **1960**, *39*, 1157−75.
(2) Lequin, R. M. Enzyme immunoassay (EIA)/enzyme-linked immunosorbent assay (ELISA). *Clin. Chem.* **2005**, *51* (12), 2415−8.
(3) Engvall, E.; Perlmann, P. Enzyme-linked immunosorbent assay (ELISA). Quantitative assay of immunoglobulin G. *Immunochemistry* **1971**, *8* (9), 871−4.
(4) Diamandis, E. P.; Morton, R. C. Time-resolved fluorescence using a europium chelate of 4,7-bis-(chlorosulfophenyl)-1,10-phenanthroline-2,9-dicarboxylic acid (BCPDA). Labeling procedures and applications in immunoassays. *J. Immunol. Methods* **1988**, *112* (1), 43−52.
(5) Aebersold, R.; Mann, M. Mass spectrometry-based proteomics. *Nature* **2003**, *422* (6928), 198−207.
(6) Kang, U. B.; Yeom, J.; Kim, H. J.; Kim, H.; Lee, C. Expression profiling of more than 3500 proteins of MSS-type colorectal cancer by stable isotope labeling and mass spectrometry. *J. Proteomics* **2012**, *75* (10), 3050−62.
(7) Kang, U. B.; Yeom, J.; Kim, H.; Lee, C. Quantitative analysis of mTRAQ-labeled proteome using full MS scans. *J. Proteome Res.* **2010**, *9* (7), 3750−8.
(8) Yu, M. J.; Pisitkun, T.; Wang, G.; Shen, R. F.; Knepper, M. A. LC−MS/MS analysis of apical and basolateral plasma membranes of rat renal collecting duct cells. *Mol. Cell. Proteomics* **2006**, *5* (11), 2131−45.
(9) Ahn, Y.; Kang, U. B.; Kim, J.; Lee, C. Mining of serum glycoproteins by an indirect approach using cell line secretome. *Mol. Cells* **2010**, *29* (2), 123−30.
(10) Bern, M.; Finney, G.; Hoopmann, M. R.; Merrihew, G.; Toth, M. J.; MacCoss, M. J. Deconvolution of mixture spectra from ion-trap data-independent-acquisition tandem mass spectrometry. *Anal. Chem.* **2010**, *82* (3), 833−41.
(11) Anderson, L.; Hunter, C. L. Quantitative mass spectrometric multiple reaction monitoring assays for major plasma proteins. *Mol. Cell. Proteomics* **2006**, *5* (4), 573−88.
(12) Brun, V.; Dupuis, A.; Adrait, A.; Marcellin, M.; Thomas, D.; Court, M.; Vandenesch, F.; Garin, J. Isotope-labeled protein standards: toward absolute quantitative proteomics. *Mol. Cell. Proteomics* **2007**, *6* (12), 2139−49.
(13) Domon, B.; Aebersold, R. Mass spectrometry and protein analysis. *Science* **2006**, *312* (5771), 212−7.
(14) Picotti, P.; Rinner, O.; Stallmach, R.; Dautel, F.; Farrah, T.; Domon, B.; Wenschuh, H.; Aebersold, R. High-throughput generation of selected reaction-monitoring assays for proteins and proteomes. *Nat. Methods* **2010**, *7* (1), 43−6.
(15) Whiteaker, J. R.; Lin, C.; Kennedy, J.; Hou, L.; Trute, M.; Sokal, I.; Yan, P.; Schoenherr, R. M.; Zhao, L.; Voytovich, U. J.; Kelly-Spratt, K. S.; Krasnoselsky, A.; Gafken, P. R.; Hogan, J. M.; Jones, L. A.; Wang, P.; Amon, L.; Chodosh, L. A.; Nelson, P. S.; McIntosh, M. W.; Kemp, C. J.; Paulovich, A. G. A targeted proteomics-based pipeline for verification of biomarkers in plasma. *Nat. Biotechnol.* **2011**, *29* (7), 625−34.
(16) Wang, Q.; Chaerkady, R.; Wu, J.; Hwang, H. J.; Papadopoulos, N.; Kopelovich, L.; Maitra, A.; Matthaei, H.; Eshleman, J. R.; Hruban, R. H.; Kinzler, K. W.; Pandey, A.; Vogelstein, B. Mutant proteins as cancer-specific biomarkers. *Proc. Natl. Acad. Sci. U. S. A.* **2011**, *108* (6), 2444−9.
(17) Lopez, M. F.; Rezai, T.; Sarracino, D. A.; Prakash, A.; Krastins, B.; Athanas, M.; Singh, R. J.; Barnidge, D. R.; Oran, P.; Borges, C.; Nelson, R. W. Selected reaction monitoring-mass spectrometric immunoassay responsive to parathyroid hormone and related variants. *Clin. Chem.* **2010**, *56* (2), 281−90.

(18) Kuzyk, M. A.; Smith, D.; Yang, J. C.; Cross, T. J.; Jackson, A. M.; Hardie, D. B.; Anderson, N. L.; Borchers, C. H. Multiple reaction monitoring-based, multiplexed, absolute quantitation of 45 proteins in human plasma. *Mol. Cell. Proteomics* **2009**, *8* (8), 1860−77.
(19) Kiyonami, R.; Schoen, A.; Prakash, A.; Peterman, S.; Zabrouskov, V.; Picotti, P.; Aebersold, R.; Huhmer, A.; Domon, B. Increased selectivity, analytical precision, and throughput in targeted proteomics. *Mol. Cell. Proteomics* **2011**, *10* (2), M110 002931.
(20) Maclean, B.; Tomazela, D. M.; Abbatiello, S. E.; Zhang, S.; Whiteaker, J. R.; Paulovich, A. G.; Carr, S. A.; Maccoss, M. J. Effect of collision energy optimization on the measurement of peptides by selected reaction monitoring (SRM) mass spectrometry. *Anal. Chem.* **2010**, *82* (24), 10116−24.
(21) American Cancer Society, Cancer Facts & Figures 2011. http://www.cancer.org/Research/CancerFactsFigures/CancerFactsFigures/cancer-facts-figures-2011 (accessed April 5, 2012).
(22) Vigano, M. G.; Cavina R.; Novello, S.; Grossi, F.; Santoro, A.; Gregorc, V.; Scagliotti, G.; Garassino, I. M.; Rossoni, G.; Levra, M. G.; Genova, C.; Caligaris-Cappio, F.; Lambiase, A.; Bordignon, C. Phase II trial of NGR-hTNF and doxorubicin in relapsed small cell lung cancer (SCLC). *J. Clin. Oncol.* **2011**, *29*, Suppl; Abstr 7077.
(23) University of Nebraska, N. C. I. N., A Phase I Study of Weekly Doxorubicin and Oral Topotecan for Patients With Relapsed or Refractory Small Cell Lung Cancer (SCLC). http://clinicaltrials.gov/ct2/show/NCT00856037 (accessed April 5, 2012).
(24) Gao, Z.; Fields, J. Z.; Boman, B. M. Co-transfection of MDR1 and MRP antisense RNAs abolishes the drug resistance in multidrug-resistant human lung cancer cells. *Anticancer Res.* **1998**, *18* (4C), 3073−6.
(25) Sharma, A.; Patrick, B.; Li, J.; Sharma, R.; Jeyabal, P. V. S.; Reddy, P. M. R. V.; Awasthi, S.; Awasthi, Y. C. Glutathione S-transferases as antioxidant enzymes: Small cell lung cancer (H69) cells transfected with hGSTA1 resist doxorubicin-induced apoptosis. *Arch. Biochem. Biophys.* **2006**, *452* (2), 165−73.
(26) Hao, X. Y.; Bergh, J.; Brodin, O.; Hellman, U.; Mannervik, B. Acquired resistance to cisplatin and doxorubicin in a small cell lung cancer cell line is correlated to elevated expression of glutathione-linked detoxification enzymes. *Carcinogenesis* **1994**, *15* (6), 1167−73.
(27) Mattern, J.; Volm, M. Increased resistance to doxorubicin in human non-small-cell lung carcinomas with metallothionein expression. *Int. J. Oncol.* **1992**, *1* (6), 687−9.
(28) Beck, M.; Schmidt, A.; Malmstroem, J.; Claassen, M.; Ori, A.; Szymborska, A.; Herzog, F.; Rinner, O.; Ellenberg, J.; Aebersold, R. The quantitative proteome of a human cell line. *Mol. Syst. Biol.* **2011**, *7*, 549.
(29) Das, S.; Bosley, A. D.; Ye, X.; Chan, K. C.; Chu, I.; Green, J. E.; Issaq, H. J.; Veenstra, T. D.; Andresson, T. Comparison of strong cation exchange and SDS-PAGE fractionation for analysis of multiprotein complexes. *J. Proteome Res.* **2010**, *9* (12), 6696−704.
(30) Geiger, T.; Clarke, S. Deamidation, isomerization, and racemization at asparaginyl and aspartyl residues in peptides. Succinimide-linked reactions that contribute to protein degradation. *J. Biol. Chem.* **1987**, *262* (2), 785−94.
(31) Yang, W. S.; Moon, H. G.; Kim, H. S.; Choi, E. J.; Yu, M. H.; Noh, D. Y.; Lee, C. Proteomic approach reveals FKBP4 and S100A9 as potential prediction markers of therapeutic response to neoadjuvant chemotherapy in patients with breast cancer. *J. Proteome Res.* **2012**, *11* (2), 1078−88.
(32) Wagner, K. W.; Punnoose, E. A.; Januario, T.; Lawrence, D. A.; Pitti, R. M.; Lancaster, K.; Lee, D.; von Goetz, M.; Yee, S. F.; Totpal, K.; Huw, L.; Katta, V.; Cavet, G.; Hymowitz, S. G.; Amler, L.; Ashkenazi, A. Death-receptor O-glycosylation controls tumor-cell sensitivity to the proapoptotic ligand Apo2L/TRAIL. *Nat. Med.* **2007**, *13* (9), 1070−7.
(33) Edgar, R.; Domrachev, M.; Lash, A. E. Gene Expression Omnibus: NCBI gene expression and hybridization array data repository. *Nucleic Acids Res.* **2002**, *30* (1), 207−10.
(34) Walpole, R. E. *Probability & Statistics for Engineers & Scientists*, 9th ed.; Prentice Hall: Boston, 2012; p 791.
(35) Tse, C.; Shoemaker, A. R.; Adickes, J.; Anderson, M. G.; Chen, J.; Jin, S.; Johnson, E. F.; Marsh, K. C.; Mitten, M. J.; Nimmer, P.; Roberts, L.; Tahir, S. K.; Xiao, Y.; Yang, X.; Zhang, H.; Fesik, S.; Rosenberg, S. H.; Elmore, S. W. ABT-263: a potent and orally bioavailable Bcl-2 family inhibitor. *Cancer Res.* **2008**, *68* (9), 3421−8.
(36) Wu, Z. J.; Irizarry, R. A.; Gentleman, R.; Martinez-Murillo, F.; Spencer, F. A model-based background adjustment for oligonucleotide expression arrays. *J. Am. Stat. Assoc.* **2004**, *99* (468), 909−17.
(37) Lee, H. J.; Suk, J. E.; Patrick, C.; Bae, E. J.; Cho, J. H.; Rho, S.; Hwang, D.; Masliah, E.; Lee, S. J. Direct transfer of alpha-synuclein from neuron to astroglia causes inflammatory responses in synucleinopathies. *J. Biol. Chem.* **2010**, *285* (12), 9262−72.
(38) Ekins, S.; Nikolsky, Y.; Bugrim, A.; Kirillov, E.; Nikolskaya, T. Pathway mapping tools for analysis of high content data. *Methods Mol. Biol.* **2007**, *356*, 319−50.
(39) Huang da, W.; Sherman, B. T.; Lempicki, R. A. Systematic and integrative analysis of large gene lists using DAVID bioinformatics resources. *Nat. Protoc.* **2009**, *4* (1), 44−57.
(40) Ashburner, M.; Ball, C. A.; Blake, J. A.; Botstein, D.; Butler, H.; Cherry, J. M.; Davis, A. P.; Dolinski, K.; Dwight, S. S.; Eppig, J. T.; Harris, M. A.; Hill, D. P.; Issel-Tarver, L.; Kasarskis, A.; Lewis, S.; Matese, J. C.; Richardson, J. E.; Ringwald, M.; Rubin, G. M.; Sherlock, G. Gene ontology: tool for the unification of biology. The Gene Ontology Consortium. *Nat. Genet.* **2000**, *25* (1), 25−9.
(41) Cline, M. S.; Smoot, M.; Cerami, E.; Kuchinsky, A.; Landys, N.; Workman, C.; Christmas, R.; Avila-Campilo, I.; Creech, M.; Gross, B.; Hanspers, K.; Isserlin, R.; Kelley, R.; Killcoyne, S.; Lotia, S.; Maere, S.; Morris, J.; Ono, K.; Pavlovic, V.; Pico, A. R.; Vailaya, A.; Wang, P. L.; Adler, A.; Conklin, B. R.; Hood, L.; Kuiper, M.; Sander, C.; Schmulevich, I.; Schwikowski, B.; Warner, G. J.; Ideker, T.; Bader, G. D. Integration of biological networks and gene expression data using Cytoscape. *Nat. Protoc.* **2007**, *2* (10), 2366−82.
(42) Ding, L.; Getz, G.; Wheeler, D. A.; Mardis, E. R.; McLellan, M. D.; Cibulskis, K.; Sougnez, C.; Greulich, H.; Muzny, D. M.; Morgan, M. B.; Fulton, L.; Fulton, R. S.; Zhang, Q.; Wendl, M. C.; Lawrence, M. S.; Larson, D. E.; Chen, K.; Dooling, D. J.; Sabo, A.; Hawes, A. C.; Shen, H.; Jhangiani, S. N.; Lewis, L. R.; Hall, O.; Zhu, Y.; Mathew, T.; Ren, Y.; Yao, J.; Scherer, S. E.; Clerc, K.; Metcalf, G. A.; Ng, B.; Milosavljevic, A.; Gonzalez-Garay, M. L.; Osborne, J. R.; Meyer, R.; Shi, X.; Tang, Y.; Koboldt, D. C.; Lin, L.; Abbott, R.; Miner, T. L.; Pohl, C.; Fewell, G.; Haipek, C.; Schmidt, H.; Dunford-Shore, B. H.; Kraja, A.; Crosby, S. D.; Sawyer, C. S.; Vickery, T.; Sander, S.; Robinson, J.; Winckler, W.; Baldwin, J.; Chirieac, L. R.; Dutt, A.; Fennell, T.; Hanna, M.; Johnson, B. E.; Onofrio, R. C.; Thomas, R. K.; Tonon, G.; Weir, B. A.; Zhao, X.; Ziaugra, L.; Zody, M. C.; Giordano, T.; Orringer, M. B.; Roth, J. A.; Spitz, M. R.; Wistuba, I. I.; Ozenberger, B.; Good, P. J.; Chang, A. C.; Beer, D. G.; Watson, M. A.; Ladanyi, M.; Broderick, S.; Yoshizawa, A.; Travis, W. D.; Pao, W.; Province, M. A.; Weinstock, G. M.; Varmus, H. E.; Gabriel, S. B.; Lander, E. S.; Gibbs, R. A.; Meyerson, M.; Wilson, R. K. Somatic mutations affect key pathways in lung adenocarcinoma. *Nature* **2008**, *455* (7216), 1069−75.
(43) Maheswaran, S.; Sequist, L. V.; Nagrath, S.; Ulkus, L.; Brannigan, B.; Collura, C. V.; Inserra, E.; Diederichs, S.; Iafrate, A. J.; Bell, D. W.; Digumarthy, S.; Muzikansky, A.; Irimia, D.; Settleman, J.; Tompkins, R. G.; Lynch, T. J.; Toner, M.; Haber, D. A. Detection of mutations in EGFR in circulating lung-cancer cells. *N. Engl. J. Med.* **2008**, *359* (4), 366−77.
(44) Marks, J. L.; Gong, Y.; Chitale, D.; Golas, B.; McLellan, M. D.; Kasai, Y.; Ding, L.; Mardis, E. R.; Wilson, R. K.; Solit, D.; Levine, R.; Michel, K.; Thomas, R. K.; Rusch, V. W.; Ladanyi, M.; Pao, W. Novel MEK1 mutation identified by mutational analysis of epidermal growth factor receptor signaling pathway genes in lung adenocarcinoma. *Cancer Res.* **2008**, *68* (14), 5524−8.
(45) Thomas, R. K.; Baker, A. C.; Debiasi, R. M.; Winckler, W.; Laframboise, T.; Lin, W. M.; Wang, M.; Feng, W.; Zander, T.; MacConaill, L.; Lee, J. C.; Nicoletti, R.; Hatton, C.; Goyette, M.; Girard, L.; Majmudar, K.; Ziaugra, L.; Wong, K. K.; Gabriel, S.; Beroukhim, R.; Peyton, M.; Barretina, J.; Dutt, A.; Emery, C.; Greulich,

H.; Shah, K.; Sasaki, H.; Gazdar, A.; Minna, J.; Armstrong, S. A.; Mellinghoff, I. K.; Hodi, F. S.; Dranoff, G.; Mischel, P. S.; Cloughesy, T. F.; Nelson, S. F.; Liau, L. M.; Mertz, K.; Rubin, M. A.; Moch, H.; Loda, M.; Catalona, W.; Fletcher, J.; Signoretti, S.; Kaye, F.; Anderson, K. C.; Demetri, G. D.; Dummer, R.; Wagner, S.; Herlyn, M.; Sellers, W. R.; Meyerson, M.; Garraway, L. A. High-throughput oncogene mutation profiling in human cancer. *Nat. Genet.* **2007**, *39* (3), 347−51.

(46) Yamamoto, H.; Shigematsu, H.; Nomura, M.; Lockwood, W. W.; Sato, M.; Okumura, N.; Soh, J.; Suzuki, M.; Wistuba, I. I.; Fong, K. M.; Lee, H.; Toyooka, S.; Date, H.; Lam, W. L.; Minna, J. D.; Gazdar, A. F. PIK3CA mutations and copy number gains in human lung cancers. *Cancer Res.* **2008**, *68* (17), 6913−21.

(47) Bass, A. J.; Watanabe, H.; Mermel, C. H.; Yu, S.; Perner, S.; Verhaak, R. G.; Kim, S. Y.; Wardwell, L.; Tamayo, P.; Gat-Viks, I.; Ramos, A. H.; Woo, M. S.; Weir, B. A.; Getz, G.; Beroukhim, R.; O'Kelly, M.; Dutt, A.; Rozenblatt-Rosen, O.; Dziunycz, P.; Komisarof, J.; Chirieac, L. R.; Lafargue, C. J.; Scheble, V.; Wilbertz, T.; Ma, C.; Rao, S.; Nakagawa, H.; Stairs, D. B.; Lin, L.; Giordano, T. J.; Wagner, P.; Minna, J. D.; Gazdar, A. F.; Zhu, C. Q.; Brose, M. S.; Cecconello, I., Jr; U., R.; Marie, S. K.; Dahl, O.; Shivdasani, R. A.; Tsao, M. S.; Rubin, M. A.; Wong, K. K.; Regev, A.; Hahn, W. C.; Beer, D. G.; Rustgi, A. K.; Meyerson, M. SOX2 is an amplified lineage-survival oncogene in lung and esophageal squamous cell carcinomas. *Nat. Genet.* **2009**, *41* (11), 1238−42.

(48) Kendall, J.; Liu, Q.; Bakleh, A.; Krasnitz, A.; Nguyen, K. C.; Lakshmi, B.; Gerald, W. L.; Powers, S.; Mu, D. Oncogenic cooperation and coamplification of developmental transcription factor genes in lung cancer. *Proc. Natl. Acad. Sci. U. S. A.* **2007**, *104* (42), 16663−8.

(49) Weir, B. A.; Woo, M. S.; Getz, G.; Perner, S.; Ding, L.; Beroukhim, R.; Lin, W. M.; Province, M. A.; Kraja, A.; Johnson, L. A.; Shah, K.; Sato, M.; Thomas, R. K.; Barletta, J. A.; Borecki, I. B.; Broderick, S.; Chang, A. C.; Chiang, D. Y.; Chirieac, L. R.; Cho, J.; Fujii, Y.; Gazdar, A. F.; Giordano, T.; Greulich, H.; Hanna, M.; Johnson, B. E.; Kris, M. G.; Lash, A.; Lin, L.; Lindeman, N.; Mardis, E. R.; McPherson, J. D.; Minna, J. D.; Morgan, M. B.; Nadel, M.; Orringer, M. B.; Osborne, J. R.; Ozenberger, B.; Ramos, A. H.; Robinson, J.; Roth, J. A.; Rusch, V.; Sasaki, H.; Shepherd, F.; Sougnez, C.; Spitz, M. R.; Tsao, M. S.; Twomey, D.; Verhaak, R. G.; Weinstock, G. M.; Wheeler, D. A.; Winckler, W.; Yoshizawa, A.; Yu, S.; Zakowski, M. F.; Zhang, Q.; Beer, D. G.; Wistuba, I. I.; Watson, M. A.; Garraway, L. A.; Ladanyi, M.; Travis, W. D.; Pao, W.; Rubin, M. A.; Gabriel, S. B.; Gibbs, R. A.; Varmus, H. E.; Wilson, R. K.; Lander, E. S.; Meyerson, M. Characterizing the cancer genome in lung adenocarcinoma. *Nature* **2007**, *450* (7171), 893−8.

(50) Rauch, T. A.; Zhong, X.; Wu, X.; Wang, M.; Kernstine, K. H.; Wang, Z.; Riggs, A. D.; Pfeifer, G. P. High-resolution mapping of DNA hypermethylation and hypomethylation in lung cancer. *Proc. Natl. Acad. Sci. U. S. A.* **2008**, *105* (1), 252−7.

(51) Shames, D. S.; Girard, L.; Gao, B.; Sato, M.; Lewis, C. M.; Shivapurkar, N.; Jiang, A.; Perou, C. M.; Kim, Y. H.; Pollack, J. R.; Fong, K. M.; Lam, C. L.; Wong, M.; Shyr, Y.; Nanda, R.; Olopade, O. I.; Gerald, W.; Euhus, D. M.; Shay, J. W.; Gazdar, A. F.; Minna, J. D. A genome-wide screen for promoter methylation in lung cancer identifies novel methylation markers for multiple malignancies. *PLoS Med.* **2006**, *3* (12), e486.

(52) Tsou, J. A.; Hagen, J. A.; Carpenter, C. L.; Laird-Offringa, I. A. DNA methylation analysis: a powerful new tool for lung cancer diagnosis. *Oncogene* **2002**, *21* (35), 5450−61.

(53) SABiosciences, a. Q. c., Functional Gene Grouping, Human Lung Cancer DNA Methylation PCR Array. http://www.sabiosciences.com/dna_methylation_product/HTML/MEAH-3040A.html#function (accessed April 5, 2012).

(54) Beer, D. G.; Kardia, S. L.; Huang, C. C.; Giordano, T. J.; Levin, A. M.; Misek, D. E.; Lin, L.; Chen, G.; Gharib, T. G.; Thomas, D. G.; Lizyness, M. L.; Kuick, R.; Hayasaka, S.; Taylor, J. M.; Iannettoni, M. D.; Orringer, M. B.; Hanash, S. Gene-expression profiles predict survival of patients with lung adenocarcinoma. *Nat. Med.* **2002**, *8* (8), 816−24.

(55) Bhattacharjee, A.; Richards, W. G.; Staunton, J.; Li, C.; Monti, S.; Vasa, P.; Ladd, C.; Beheshti, J.; Bueno, R.; Gillette, M.; Loda, M.; Weber, G.; Mark, E. J.; Lander, E. S.; Wong, W.; Johnson, B. E.; Golub, T. R.; Sugarbaker, D. J.; Meyerson, M. Classification of human lung carcinomas by mRNA expression profiling reveals distinct adenocarcinoma subclasses. *Proc. Natl. Acad. Sci. U. S. A.* **2001**, *98* (24), 13790−5.

(56) Garber, M. E.; Troyanskaya, O. G.; Schluens, K.; Petersen, S.; Thaesler, Z.; Pacyna-Gengelbach, M.; van de Rijn, M.; Rosen, G. D.; Perou, C. M.; Whyte, R. I.; Altman, R. B.; Brown, P. O.; Botstein, D.; Petersen, I. Diversity of gene expression in adenocarcinoma of the lung. *Proc. Natl. Acad. Sci. U. S. A.* **2001**, *98* (24), 13784−9.

(57) Jones, M. H.; Virtanen, C.; Honjoh, D.; Miyoshi, T.; Satoh, Y.; Okumura, S.; Nakagawa, K.; Nomura, H.; Ishikawa, Y. Two prognostically significant subtypes of high-grade lung neuroendocrine tumours independent of small-cell and large-cell neuroendocrine carcinomas identified by gene expression profiles. *Lancet* **2004**, *363* (9411), 775−81.

(58) Landi, M. T.; Dracheva, T.; Rotunno, M.; Figueroa, J. D.; Liu, H.; Dasgupta, A.; Mann, F. E.; Fukuoka, J.; Hames, M.; Bergen, A. W.; Murphy, S. E.; Yang, P.; Pesatori, A. C.; Consonni, D.; Bertazzi, P. A.; Wacholder, S.; Shih, J. H.; Caporaso, N. E.; Jen, J. Gene expression signature of cigarette smoking and its role in lung adenocarcinoma development and survival. *PLoS One* **2008**, *3* (2), e1651.

(59) Zhou, B. B.; Peyton, M.; He, B.; Liu, C.; Girard, L.; Caudler, E.; Lo, Y.; Baribaud, F.; Mikami, I.; Reguart, N.; Yang, G.; Li, Y.; Yao, W.; Vaddi, K.; Gazdar, A. F.; Friedman, S. M.; Jablons, D. M.; Newton, R. C.; Fridman, J. S.; Minna, J. D.; Scherle, P. A. Targeting ADAM-mediated ligand cleavage to inhibit HER3 and EGFR pathways in non-small cell lung cancer. *Cancer Cell* **2006**, *10* (1), 39−50.

(60) Huang, L. J.; Chen, S. X.; Huang, Y.; Luo, W. J.; Jiang, H. H.; Hu, Q. H.; Zhang, P. F.; Yi, H. Proteomics-based identification of secreted protein dihydrodiol dehydrogenase as a novel serum markers of non-small cell lung cancer. *Lung Cancer* **2006**, *54* (1), 87−94.

(61) Planque, C.; Kulasingam, V.; Smith, C. R.; Reckamp, K.; Goodglick, L.; Diamandis, E. P. Identification of five candidate lung cancer biomarkers by proteomics analysis of conditioned media of four lung cancer cell lines. *Mol. Cell. Proteomics* **2009**, *8* (12), 2746−58.

(62) Rikova, K.; Guo, A.; Zeng, Q.; Possemato, A.; Yu, J.; Haack, H.; Nardone, J.; Lee, K.; Reeves, C.; Li, Y.; Hu, Y.; Tan, Z.; Stokes, M.; Sullivan, L.; Mitchell, J.; Wetzel, R.; Macneill, J.; Ren, J. M.; Yuan, J.; Bakalarski, C. E.; Villen, J.; Kornhauser, J. M.; Smith, B.; Li, D.; Zhou, X.; Gygi, S. P.; Gu, T. L.; Polakiewicz, R. D.; Rush, J.; Comb, M. J. Global survey of phosphotyrosine signaling identifies oncogenic kinases in lung cancer. *Cell* **2007**, *131* (6), 1190−203.

(63) Tian, T.; Hao, J.; Xu, A.; Luo, C.; Liu, C.; Huang, L.; Xiao, X.; He, D. Determination of metastasis-associated proteins in non-small cell lung cancer by comparative proteomic analysis. *Cancer Sci.* **2007**, *98* (8), 1265−74.

(64) Tyan, Y. C.; Wu, H. Y.; Lai, W. W.; Su, W. C.; Liao, P. C. Proteomic profiling of human pleural effusion using two-dimensional nano liquid chromatography tandem mass spectrometry. *J. Proteome Res.* **2005**, *4* (4), 1274−86.

(65) Xiao, T.; Ying, W.; Li, L.; Hu, Z.; Ma, Y.; Jiao, L.; Ma, J.; Cai, Y.; Lin, D.; Guo, S.; Han, N.; Di, X.; Li, M.; Zhang, D.; Su, K.; Yuan, J.; Zheng, H.; Gao, M.; He, J.; Shi, S.; Li, W.; Xu, N.; Zhang, H.; Liu, Y.; Zhang, K.; Gao, Y.; Qian, X.; Cheng, S. An approach to studying lung cancer-related proteins in human blood. *Mol. Cell. Proteomics* **2005**, *4* (10), 1480−6.

(66) Huillet, C.; Adrait, A.; Lebert, D.; Picard, G.; Trauchessec, M.; Louwagie, M.; Dupuis, A.; Hittinger, L.; Ghaleb, B.; Le Corvoisier, P.; Jaquinod, M.; Garin, J.; Bruley, C.; Brun, V. Accurate quantification of cardiovascular biomarkers in serum using Protein Standard Absolute Quantification (PSAQ) and selected reaction monitoring. *Mol. Cell. Proteomics* **2012**, *11* (2), M111 008235.

(67) de Sousa Abreu, R.; Penalva, L. O.; Marcotte, E. M.; Vogel, C. Global signatures of protein and mRNA expression levels. *Mol. Biosyst.* **2009**, *5* (12), 1512−26.

(68) Khodarev, N. N.; Roach, P.; Pitroda, S. P.; Golden, D. W.; Bhayani, M.; Shao, M. Y.; Darga, T. E.; Beveridge, M. G.; Sood, R. F.; Sutton, H. G.; Beckett, M. A.; Mauceri, H. J.; Posner, M. C.; Weichselbaum, R. R. STAT1 pathway mediates amplification of metastatic potential and resistance to therapy. *PLoS One* **2009**, *4* (6), e5821.
(69) Rickardson, L.; Fryknas, M.; Dhar, S.; Lovborg, H.; Gullbo, J.; Rydaker, M.; Nygren, P.; Gustafsson, M. G.; Larsson, R.; Isaksson, A. Identification of molecular mechanisms for cellular drug resistance by combining drug activity and gene expression profiles. *Br. J. Cancer* **2005**, *93* (4), 483−92.
(70) Wang, B.; Hsu, S. H.; Majumder, S.; Kutay, H.; Huang, W.; Jacob, S. T.; Ghoshal, K. TGFbeta-mediated upregulation of hepatic miR-181b promotes hepatocarcinogenesis by targeting TIMP3. *Oncogene* **2010**, *29* (12), 1787−97.
(71) Tang, X.; Gao, J. S.; Guan, Y. J.; McLane, K. E.; Yuan, Z. L.; Ramratnam, B.; Chin, Y. E. Acetylation-dependent signal transduction for type I interferon receptor. *Cell* **2007**, *131* (1), 93−105.
(72) Burkard, T. R.; Planyavsky, M.; Kaupe, I.; Breitwieser, F. P.; Burckstummer, T.; Bennett, K. L.; Superti-Furga, G.; Colinge, J. Initial characterization of the human central proteome. *BMC Syst. Biol.* **2011**, *5*, 17.
(73) Fonslow, B. R.; Stein, B. D.; Webb, K. J.; Xu, T.; Choi, J.; Park, S. K.; Yates, J. R., 3rd Digestion and depletion of abundant proteins improves proteomic coverage. *Nat. Methods* **2013**, *10* (1), 54−6.
(74) Glatter, T.; Ludwig, C.; Ahrne, E.; Aebersold, R.; Heck, A. J.; Schmidt, A. Large-scale quantitative assessment of different in-solution protein digestion protocols reveals superior cleavage efficiency of tandem Lys-C/trypsin proteolysis over trypsin digestion. *J. Proteome Res.* **2012**, *11* (11), 5145−56.
(75) Dycka, F.; Bobal, P.; Mazanec, K.; Bobalova, J. Rapid and efficient protein enzymatic digestion: an experimental comparison. *Electrophoresis* **2012**, *33* (2), 288−95.